Mixed $\mathcal{H}_2/\mathcal{H}_\infty$ Observer-Based LPV Control of a Hydraulic Engine Cam Phasing Actuator

Andrew White, *Student Member, IEEE*, Zhen Ren, Guoming Zhu, and Jongeun Choi

***Abstract*—In this paper, a family of linear models previously obtained from a series of closed-loop system identification tests for a variable valve timing cam phaser system is used to design a dynamic gain-scheduling controller. Using engine speed and oil pressure as the scheduling parameters, the family of linear models was translated into a linear parameter varying (LPV) system. An observer-based gain-scheduling controller for the LPV system is then designed based on the linear matrix inequality technique. A discussion on weighting function selection for mixed $\mathcal{H}_2/\mathcal{H}_\infty$ controller synthesis is presented, with an emphasis placed on examining various frequency responses of the system. Test bench results show the effectiveness of the proposed scheme.**

***Index Terms*—Engine and powertrain control, gain-scheduling control, hydraulic control system, linear parameter varying (LPV) control, robust control.**

I. Introduction

THE intake and exhaust valve timing of an internal combustion (IC) engine greatly influence the fuel economy, emissions, and performance of an IC engine. Conventional valvetrain systems can only optimize the intake and exhaust valve timing for one given operational condition. That is, the optimized valve timing can either improve fuel economy and reduce emissions at low engine speeds or maximize engine power and torque outputs at high engine speeds. However, with the development of continuously variable valve timing (VVT) systems [1], the intake and exhaust valve timing can be modified as a function of engine speed and load to obtain both improved fuel economy and reduced emissions at low engine speeds and increased power and torque at high engine speeds.

To adjust the intake and exhaust timing, the most common cam phasing system is the hydraulic van type cam phaser [2]. The control of hydraulic cam phasing systems has been discussed in [3] and [4]. In [3], a significant nonlinearity in the hydraulic cam phasing system is noted and a nonlinear controller is designed to compensate for it. In [4], an $\mathcal{H}_2$ controller is designed using the output covariance constraint (OCC) control design approach [5]. In this paper, a gain-scheduling controller is developed using linear parameter varying (LPV) control design.

Manuscript received July 29, 2011; accepted November 12, 2011. Manuscript received in final form November 17, 2011. Date of publication December 13, 2011; date of current version December 14, 2012. Recommended by Associate Editor U. Christen. This work was supported in part by the U.S. Department of Energy under Grant DE-FC26-07NT43275.

A. White and Z. Ren are with the Department of Mechanical Engineering, Michigan State University, East Lansing, MI 48824 USA (e-mail: whitea23@egr.msu.edu; renzhen@egr.msu.edu).

G. Zhu and J. Choi are with the Department of Mechanical Engineering and the Department of Electrical Engineering, Michigan State University, East Lansing, MI 48824 USA (e-mail: zhug@egr.msu.edu; jchoi@egr.msu.edu).

Digital Object Identifier 10.1109/TCST.2011.2177464

In recent years, the use of LPV modeling and control in automotive applications has received a great deal of attention. LPV modeling and control techniques have been applied to both diesel engines [6], [7] and gasoline spark-ignition engines [8]–[11]. In [6], LPV control techniques are applied to the air path of turbocharged diesel engines to control the transient exhaust gas fraction pumped into the cylinders to reduce nitrous oxide emissions. In [7], an LPV identification technique is applied to a nonlinear turbocharged diesel engine to obtain an LPV model suitable for control synthesis. In [8], a continuous-time LPV model is developed considering only engine speed as a time-varying parameter. In [9], a large variable time delay is present in the air-fuel ratio control loop for a lean burn spark ignition engine. LPV control methods are used to compensate for the variable time delay. In [10] and [11], event-based gain-scheduling proportional-integral (PI) and proportional-integral-derivative (PID) controllers are developed using the wall-wetting parameters and engine speed as time-varying parameters. In this paper, the techniques used in [10] and [11] to obtain the static PI and PID gain-scheduling controllers are augmented to develop an observer-based dynamic LPV controller using the dynamics of the plant.

To obtain the model of the VVT system, closed-loop system identification was used in [4] and [12]. A main reason for selecting closed-loop system identification in [4] and [12] was due to high open-loop gains that makes it difficult to maintain the cam phaser operated at a fixed location for system identification. During the system identification process, it was found that the system gain of the VVT actuator is a function of engine speed, load, oil pressure, and temperature. Therefore, it seems only natural to exploit the knowledge of how the system gain of the VVT actuator varies with the time varying parameters. To do this, the VVT system can be described as a family of linear models to approximate the system dynamics for a given engine speed, load, oil pressure, and temperature. Thus formulating an LPV model for the VVT system.

The purpose of this paper is to develop a dynamic gain-scheduling controller with guaranteed stability and performance over all time-varying parameters. To do this, the process depicted in Fig. 1 was followed. First, a family of linear-time-invariant (LTI) models was obtained. Using engine speed and the oil pressure as system parameters, a family of linear models of the VVT system were obtained by performing multiple system identifications while maintaining engine speed and oil pressure at specified levels. With the family of linear models, the LPV model of the VVT system was formulated. To design the dynamic gain-scheduling controller, a standard control structure of observer-based state feedback with integral control was employed. This control structure, along with $\mathcal{H}_2$ and $\mathcal{H}_\infty$ performance weighting functions, were then appended onto the

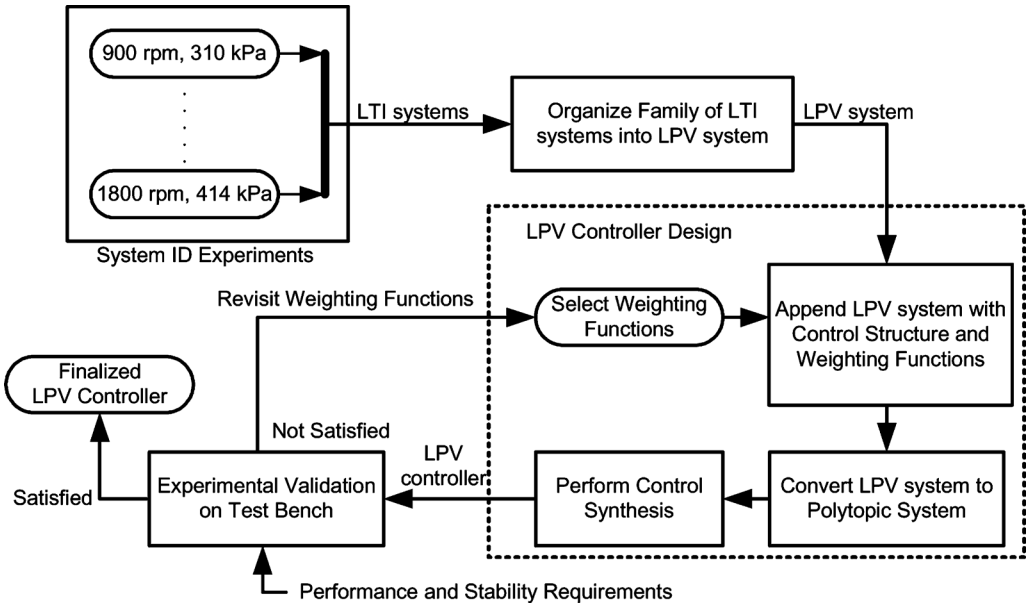

Fig. 1. Flowchart of the design and validation process of an LPV controller.

LPV model of the VVT system to obtain the LPV system of the generalized plant. Then the LPV system of the generalized plant was converted to a polytopic system, which is an LPV system with a polytopic dependency on a scheduling parameter that takes values in the unit-simplex, so that the mixed $\mathcal{H}_2/\mathcal{H}_\infty$ discrete-time LPV control synthesis method given by [13] could be applied to obtain the gain-scheduled state feedback and observer gains. Once a potential controller was obtained, its performance was experimentally validated on the test bench used to obtain the family of LTI systems. If the performance and stability requirements of the VVT system are not satisfied when testing the LPV controller, the selected $\mathcal{H}_2$ and $\mathcal{H}_\infty$ performance weighting functions are modified and the control synthesis procedure is performed again. This loop is performed until stability and satisfactory performance are obtained on the test bench.

As stated previously, a multi-objective, mixed $\mathcal{H}_2/\mathcal{H}_\infty$ control design is performed in this paper. The goal of using both $\mathcal{H}_2$ and $\mathcal{H}_\infty$ performance criteria is to design a controller which can meet multiple performance objectives. In this paper, a loose $\mathcal{H}_\infty$ performance bound is used to guarantee stability of the closed-loop system under parameter variations. Meanwhile, a tight $\mathcal{H}_2$ performance bound is used to make the LPV controller robust to input disturbances. The selection of $\mathcal{H}_2$ and $\mathcal{H}_\infty$ performance weighting functions is an important design problem. The selection of $\mathcal{H}_\infty$ performance weighting functions can be done as described in [14] and [15]. However, the selection of $\mathcal{H}_2$ performance weighting functions is not covered in such detail. In [5], a systematic way is provided for iteratively tuning the output $\mathcal{H}_2$ weighting functions for robust control of LTI systems. Unfortunately, no such iterative procedure exist yet for LPV systems.

This paper is organized as follows. The family of linear models obtained from the series of bench identification tests are introduced in Section II and the LPV system is formulated. In Section III, the LPV gain-scheduling controller design method is provided. The bench test setup is discussed in Section IV-A. In Section IV-B, the obtained LPV gain-scheduling controller is operated on the test bench and compared to the baseline PI and OCC controllers used in [12]. Concluding remarks are given in the final section.

II. LPV System Modeling

To obtain a family of linear models, the closed-loop system identification outlined in [12] was performed at a series of fixed engine speeds N and oil pressures p. The open-loop transfer functions of the identified family of linear VVT systems sampled at 5 ms are given by

$$\begin{aligned} G(N, p = 310\,\mathrm{kPa}) &= \frac{\Psi(N,p)\,(0.0859q - 0.0609)}{q^2 - 1.9547q + 0.9553} \\ G(N, p = 414\,\mathrm{kPa}) &= \frac{\Psi(N,p)\,(0.0615q - 0.0364)}{q^2 - 1.9547q + 0.9553} \end{aligned} \quad (1)$$

where $\Psi(N,p)$ is the gain at a specific engine speed N and oil pressure p as given in Table I and q is the *forward shift operator* that satisfies $qu(k) = u(k+1)$.

By inspection of the identified transfer functions in (1), the LPV model for the VVT system is given by

$$G(\alpha_k, \beta_k) = \frac{\alpha_k q + \beta_k}{q^2 - 1.9547q + 0.9553} \quad (2)$$

where α_k and β_k are used as the time-varying parameters. For notational simplicity, α_k and β_k will be used to denote the parameters at time k, such that $\alpha_k = \alpha(k)$ and $\beta_k = \beta(k)$. The values of α_k and β_k are found for a specific value of engine speed N and oil pressure p by multiplying the appropriate Ψ value found in Table I with the appropriate transfer function in 1. The range of values that α_k and β_k can take are given in Table II.

TABLE I
IDENTIFIED GAIN $\Psi(N,p)$

Pressure, p (kPa)	Engine Speed, N (rpm)	Gain $\Psi(N,p)$
310	900	0.70
	1500	0.72
	1800	0.68
414	900	0.95
	1500	0.98
	1800	0.93

TABLE II
TIME-VARYING PARAMETERS (SCHEDULING PARAMETERS)

$\alpha(N(t),p(t)) \in [0.0571, 0.0618]$
$\beta(N(t),p(t)) \in [-0.0438, -0.0339]$

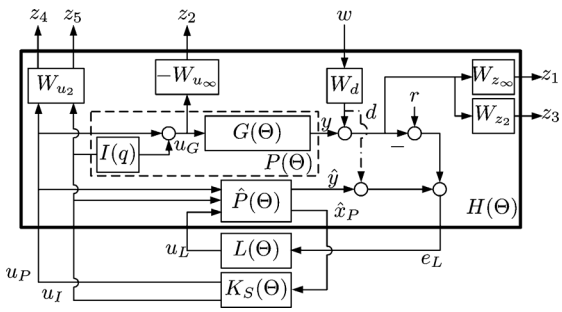

Fig. 2. Proposed control architecture for the VVT system.

Using the transfer function in (2), a state-space representation of the VVT system is found to be

$$x_G(k+1) = \underbrace{\begin{bmatrix} 0 & -0.9553 \\ 1 & 1.9547 \end{bmatrix}}_{A_G} x_G(k) + \underbrace{\begin{bmatrix} \beta_k \\ \alpha_k \end{bmatrix}}_{B_G} u_G(k),$$
$$y(k) = \underbrace{\begin{bmatrix} 0 & 1 \end{bmatrix}}_{C_G} x_G(k). \tag{3}$$

For convenience, the compact notation $\Theta = [\alpha_k, \beta_k]$ will be used to denote the scheduling variables for the remainder of this paper.

III. LPV GAIN SCHEDULING CONTROLLER DESIGN

A. Control Strategy

The objective of the control system is to regulate the cam phase y to a reference phase r using feedback control against the disturbance signal d and the time-varying parameters α_k and β_k. In particular, we want to guarantee the stability of the closed-loop system and also minimize the effect of the disturbances for any conceivable engine speed and oil pressure variations. The proposed control architecture is illustrated in Fig. 2. This scheme has four components, that is a state observer $\hat{P}(\Theta)$, observer gains $L(\Theta)$, a state feedback controller $K_S(\Theta)$, and an integrator $I(q)$.

The multi-input, single-output LPV plant $P(\Theta)$, depicted inside of the dotted box in Fig. 2, is obtained by augmenting the VVT system $G(\Theta)$ with the forward Euler method, discrete-time integrator $I(q) = t_s/(q-1)$, where t_s is the sample period of the discrete-time system in seconds. The integrator $I(q)$ introduces integral action into the system to ensure that the steady-state error between the measured cam phase y and the reference phase r can be eliminated. By allowing the input to the VVT plant $G(\Theta)$ to be equal to

$$u_G(k) = u_P(k) + \frac{t_s}{q-1} u_I(k)$$

as displayed in the dotted box of Fig. 2, one possible state-space representation of $P(\Theta)$ is found to be

$$x_P(k+1) = \underbrace{\begin{bmatrix} 0 & -0.9553 & \sqrt{t_s}\beta_k \\ 1 & 1.9547 & \sqrt{t_s}\alpha_k \\ 0 & 0 & 1 \end{bmatrix}}_{A_P(\Theta)} x_P(k) + \underbrace{\begin{bmatrix} \beta_k & 0 \\ \alpha_k & 0 \\ 0 & \sqrt{t_s} \end{bmatrix}}_{B_P(\Theta)} \underbrace{\begin{bmatrix} u_P(k) \\ u_I(k) \end{bmatrix}}_{u_S(k)}$$
$$y(k) = \underbrace{\begin{bmatrix} 0 & 1 & 0 \end{bmatrix}}_{C_P} x_P(k). \tag{4}$$

In (4), it is clear that the state matrix $A_P(\Theta)$ and the input matrix $B_P(\Theta)$ are both affected by the time-varying parameters α_k and β_k.

The state observer $\hat{P}(\Theta)$ is used to obtain the estimated states $\hat{x}_P$ of the plant. The observer $\hat{P}(\Theta)$ has the standard state-space representation

$$\hat{x}_P(k+1) = A_P(\Theta)\hat{x}_P(k) + B_P(\Theta)u_S(k) + L(\Theta)e_L(k)$$
$$\hat{y}(k) = C_P\hat{x}_P(k)$$

where the error input to the plant observer is given by $e_L(k) = r(k) - (y(k) + d(k)) + (\hat{y}(k) + d(k))$, which simplifies to $e_L(k) = r(k) - y(k) + \hat{y}(k)$. Since we are solving the S/KS mixed-sensitivity $\mathcal{H}_\infty$ optimization using the regulation form, during control synthesis we let the set point r equal zero as shown in [15], thus further simplifying the observer input error to $e_L(k) = -y(k) + \hat{y}(k)$. This satisfies the condition in [13] that the measurement for control is not corrupted by the exogenous input $w(k)$. Notice in Fig. 2 that the output disturbance $d(k)$ is connected to the estimated plant output $\hat{y}(k)$ by dashed-dotted lines. This is to signify that the exogenous input $d(k)$ is only available to the observer during control synthesis. However, during implementation since the output disturbance $d(k)$ cannot be measured it is not available to the observer.

To use mixed $\mathcal{H}_2/\mathcal{H}_\infty$ norms as the performance criteria for shaping the frequency response of the closed-loop system, weighting matrices (which can be considered control design parameters) are introduced in Fig. 2. Oftentimes, the weighting matrices are chosen as frequency dependent functions; however, for this problem static weighting matrices sufficed. The weighting matrix W_d was selected to model the signal d using the signal based approach discussed in [15]. The $\mathcal{H}_\infty$ performance weighting functions W_{z_∞} and W_{u_∞} were selected to limit the maximum magnitude of the sensitivity function $|S(j\omega)|$ and the controller multiplied by the sensitivity function $|KS(j\omega)|$ as discussed in [14]. In this study, the $\mathcal{H}_\infty$ performance weighting functions were selected primarily for LPV

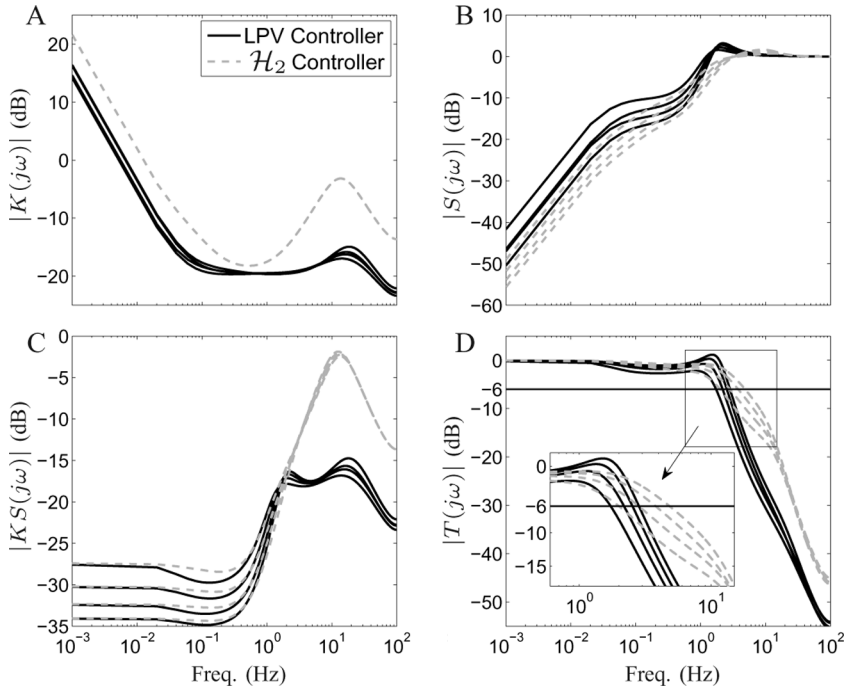

Fig. 3. Frequency response comparison of the mixed $\mathcal{H}_2/\mathcal{H}_\infty$ dynamic LPV controller with an OCC ($\mathcal{H}_2$) controller [4] at the corner points of the parameter space polytope.

stability. However, the $\mathcal{H}_2$ performance weighting functions were selected for LPV performance. The weighting matrices W_{z_2} and W_{u_2} were selected using an iterative trial-and-error process. In the iterative process, W_{z_2} and W_{u_2} started out with values of unity. The control synthesis procedure outlined in Algorithm 1 was then carried out and the sensitivity function was computed and examined. The values used in the weighting function W_{u_2} were then increased and the control synthesis was carried out again and the sensitivity function was examined again. This procedure was executed until desirable characteristics were displayed in the frequency response of the controller, the sensitivity function, and the controller multiplied by the sensitivity function. The resulting weighting matrices are as follows:

$$W_d = 1 \quad W_{u_\infty} = 10 \quad W_{u_2} = \begin{bmatrix} 15 & 0 \\ 0 & 15 \end{bmatrix} \quad W_{z_\infty} = 1$$

and $W_{z_2} = 1$. These weighting matrices where tuned to obtain the frequency responses plotted with the bold lines in Fig. 3. For comparison, a full-order dynamic output covariance constraint (OCC) controller (dashed lines) [4] was used. This controller is known to work well on the VVT cam phaser test bench at the fixed operational condition of 1500 rpm and 414 kPa oil pressure, so it was deemed an appropriate starting point.

In Fig. 3, the frequency responses of the LPV controller and the OCC controller are displayed at the corner points of the parameter space polytope (i.e., $[\underline{\alpha}, \underline{\beta}]$, $[\underline{\alpha}, \overline{\beta}]$, $[\overline{\alpha}, \underline{\beta}]$, $[\overline{\alpha}, \overline{\beta}]$, where $\underline{\alpha} = \alpha_{\min}$ and $\overline{\alpha} = \alpha_{\max}$). In Fig. 3(a), the frequency response of each controller is displayed. At low frequencies, each controller has high gain due to the integral action built into each controller. In Fig. 3(b), the sensitivity function of each controller is displayed. In a typical feedback system, the sensitivity function is linked to the tracking error performance [14]. At low frequencies, each controller's sensitivity function is small, which minimizes tracking error and maximizes disturbance rejection. Fig. 3(c) displays the frequency response of the controller multiplied by the sensitivity function for each controller. This plot shows that over the frequency range of 1–20 Hz the mixed $\mathcal{H}_2/\mathcal{H}_\infty$ dynamic LPV controller has lower control effort than the full-order dynamic OCC controller. Since this is the frequency range over which the output disturbance $d(k)$ is generally active, it means that the mixed $\mathcal{H}_2/\mathcal{H}_\infty$ dynamic LPV controller should be robust to the disturbance $d(k)$. The frequency response of the closed-loop transfer functions with the mixed $\mathcal{H}_2/\mathcal{H}_\infty$ dynamic LPV controller and the OCC controller are displayed in Fig. 3(d). The benefit of the mixed $\mathcal{H}_2/\mathcal{H}_\infty$ dynamic LPV controller can be seen in the close-up view in Fig. 3(d). At -6 dB, the closed-loop bandwidth with the OCC controller varies between approximately 2 to 4.8 Hz. However, the closed-loop bandwidth with the LPV controller only varies between approximately 1.8 to 2.9 Hz, which is a reduction in span of about 60%.

As displayed in Fig. 2, the state feedback gains $K_S(\Theta)$ and the observer gains $L(\Theta)$ are placed outside of the solid, bold box. This designates that the control synthesis in Algorithm 1 is performed on only the items inside of the box. By isolating the static gains $K_S(\Theta)$ and $L(\Theta)$, the design of the observer-based dynamic controller is transformed into the design of a single static controller $K(\Theta)$ by using the following structure:

$$\underbrace{\begin{bmatrix} u_S(k) \\ u_L(k) \end{bmatrix}}_{u(k)} = \underbrace{\begin{bmatrix} K_S(\Theta) & 0 \\ 0 & L(\Theta) \end{bmatrix}}_{K(\Theta)} \underbrace{\begin{bmatrix} \hat{x}_P(k) \\ e_L(k) \end{bmatrix}}_{e(k)} \tag{5}$$

where $\hat{x}_p \in \mathbb{R}^s$, $e_L \in \mathbb{R}$, $u_S \in \mathbb{R}^2$, and $u_L \in \mathbb{R}^s$.

B. Generalized Plant

As shown in Fig. 2, the state feedback controller $K_S(\Theta)$ and observer gains $L(\Theta)$ are designed for the generalized LPV plant $H(\Theta)$. The generalized LPV plant $H(\Theta)$ is composed by the multi-input, single-output LPV plant $P(\Theta)$ and its corresponding state observer $\hat{P}(\Theta)$, along with the static weighting matrices W_d, W_{u_∞}, W_{u_2}, W_{z_∞}, and W_{z_2}. The state-space realization of the generalized plant $H(\Theta)$ is found by combining the state-space realizations of $P(\Theta)$ and $\hat{P}(\Theta)$ and performing the connections in Fig. 2 to obtain

$$\begin{aligned}\underbrace{\begin{bmatrix} x_P(k+1) \\ \hat{x}_P(k+1) \end{bmatrix}}_{x(k+1)} &= \underbrace{\begin{bmatrix} A_P(\Theta) & 0 \\ 0 & A_P(\Theta) \end{bmatrix}}_{\hat{A}(\Theta)} \underbrace{\begin{bmatrix} x_P(k) \\ \hat{x}_P(k) \end{bmatrix}}_{x(k)} \\ &\quad + \underbrace{\begin{bmatrix} B_P(\Theta) & 0 \\ B_P(\Theta) & I \end{bmatrix}}_{\hat{B}(\Theta)} \underbrace{\begin{bmatrix} u_S(k) \\ u_L(k) \end{bmatrix}}_{u(k)} \\ z(k) &= C_z x(k) + D_w w(k) + D_u u(k) \\ e(k) &= C_e x(k) \end{aligned} \tag{6}$$

where $x(k) \in \mathbb{R}^n$ is the state at time k, $w(k) \in \mathbb{R}^r$ is the unweighted exogenous input, $u(k) \in \mathbb{R}^m$ is the control input, $z(k) \in \mathbb{R}^p$ is the performance output, and $e(k) \in \mathbb{R}^q$ is the measurement for control. The state matrix $A_P(\Theta)$ and the input matrix $B_P(\Theta)$ are both given in (4) and the other state-space matrices are given in Appendix A.

C. A Gain-Scheduling Control Synthesis Problem

Now that the state-space representation of the generalized plant $H(\Theta)$ has been obtained, the mixed $\mathcal{H}_2/\mathcal{H}_\infty$ gain-scheduling controller $K(\Theta)$ must be synthesized. The $\mathcal{H}_\infty$-norm from $w(k)$ to $\mathcal{Z}_\infty = [z_1, z_2]^\mathsf{T}$ of the LPV system $H(\Theta)$ in (6) with the gain-scheduling controller is defined as

$$\|H(\Theta)\|_\infty = \sup_{\Theta \in \boldsymbol{\Theta}, \|w\|_{\ell_2} \neq 0} \frac{\|\mathcal{Z}_\infty\|_{\ell_2}}{\|w\|_{\ell_2}}. \tag{7}$$

The $\mathcal{H}_2$-norm from $w(k)$ to $\mathcal{Z}_2 = [z_3(k), z_4(k), z_5(k)]^\mathsf{T}$ of the LPV system $H(\Theta)$ with the gain-scheduling controller is defined as

$$\|H(\Theta)\|_2^2 = \lim_{T \to \infty} \sup \mathcal{E} \left\{ \frac{1}{T} \sum_{k=0}^{T} \mathcal{Z}_2 \mathcal{Z}_2^\mathsf{T} \right\} \tag{8}$$

where $\mathcal{E}$ denotes the expectation operator and the positive integer T denotes the time horizon. Now we formally state the gain-scheduling control design problem.

1) Problem: The goal is to design a static gain-scheduling control $u(k) = K(\Theta)e(k)$ that stabilizes the closed-loop system and minimizes the worst-case $\mathcal{H}_\infty$ and $\mathcal{H}_2$ norms of the closed-loop LPV system in (7) and (8) for any trajectories of $\Theta(k) \in \boldsymbol{\Theta}$.

The gain-scheduling method provided by [13] was derived for discrete-time polytopic time-varying systems. Therefore, in the next section, the state-space representation of $H(\Theta)$ in (6) will be transformed into a polytopic time-varying system so that the controller $K(\Theta)$ can be synthesized.

D. Polytopic Linear Time-Varying System

The state-space representation of the generalized plant $H(\Theta)$ in (6) can be converted into a discrete-time polytopic time-varying system by solving the state matrix $\hat{A}(\Theta)$ and the input matrix $\hat{B}(\Theta)$ at the vertices of the parameter space polytope, e.g., the state matrix at vertice $\mathcal{V}_2$ is given by $A_2 = \hat{A}(\Theta = [\underline{\alpha}, \overline{\beta}])$. Any Θ inside of the convex parameter set is represented by a convex combination of the vertex systems as weighted by the vector $\lambda(k)$ of barycentric coordinates. Barycentric coordinates are used to specify the location of a point as the center of mass, or barycenter, of masses placed at the vertices of a simplex. A formula for computing the barycentric coordinates for any convex polytope is provided by [16]. The discrete-time polytopic time-varying system is given by

$$\begin{aligned} x(k+1) &= A(\lambda(k))x(k) + B_u(\lambda(k))u(k) \\ z(k) &= C_z x(k) + D_w w(k) + D_u u(k) \\ e(k) &= C_e x(k) \end{aligned} \tag{9}$$

where the state matrix $A(\lambda(k)) \in \mathbb{R}^{n \times n}$ and the input matrix $B(\lambda(k)) \in \mathbb{R}^{n \times m}$ belong to the polytope

$$\begin{aligned} \mathcal{D} = \Bigg\{ &(A, B_u)(\lambda(k)) : (A, B_u)(\lambda(k)) \\ &= \sum_{i=1}^{4} \lambda_i(k)(A, B_u)_i, \lambda(k) \in \Lambda \Bigg\} \end{aligned} \tag{10}$$

and the other state-space matrices are the same as in (6). The state matrix $A(\lambda(k))$ and the input matrix $B_u(\lambda(k))$ are the weighted summation of the vertex matrices as weighted by the vector $\lambda(k)$ of barycentric coordinates, i.e.,

$$\begin{aligned} A(\lambda(k)) &= \sum_{i=1}^{4} \lambda_i(k) A_i \quad \text{and} \\ B_u(\lambda(k)) &= \sum_{i=1}^{4} \lambda_i(k) B_i \end{aligned}$$

where A_i and B_i are the vertices of the polytope and $\lambda(k) \in \mathbb{R}^4$ is the barycentric coordinate vector which exists in the unit simplex

$$\Lambda = \left\{ \zeta \in \mathbb{R}^4 : \sum_{i=1}^{4} \zeta_i = 1, \zeta_i \geq 0, i = 1, \ldots, 4 \right\}. \tag{11}$$

For all $k \in \mathbb{Z}_{\geq 0}$, the rate of variation of the barycentric coordinates $\Delta\lambda_i(k) = \lambda_i(k+1) - \lambda_i(k)$, is limited such that $-b \leq \Delta\lambda_i(k) \leq b$, with $b \in [0, 1]$, which should be selected with the application in mind. If a worst-case set of parameter variation is known, then this bound can be calculated.

A finite set of LMIs in [13] can be used to design the $\mathcal{H}_2/\mathcal{H}_\infty$ gain-scheduling controller $K(\Theta)$ in (5). Due to Theorems 8 and 9 of [13], if there exists for $i = 1, \ldots, 4$, matrices $G_{i,K_s} \in \mathbb{R}^{s \times s}$, $G_{i,L} \in \mathbb{R}^{(q-s) \times (q-s)}$, $Z_{i,K_s} \in \mathbb{R}^{(m-s) \times s}$, and $Z_{i,L} \in \mathbb{R}^{s \times 1}$ assembled as

$$G_{i,1} = \begin{bmatrix} G_{i,K_s} & 0 \\ 0 & G_{i,L} \end{bmatrix}, Z_{i,1} = \begin{bmatrix} Z_{i,K_s} & 0 \\ 0 & Z_{i,L} \end{bmatrix} \tag{12}$$

along with the other matrix variables defined in Theorems 8 and 9 of [13] satisfying the $\mathcal{H}_\infty$ LMIs and the $\mathcal{H}_2$ LMIs in [13], then the $\mathcal{H}_2/\mathcal{H}_\infty$ controller $K(\lambda(k))$ is given by

$$K(\lambda(k)) = \hat{Z}(\lambda(k))\hat{G}(\lambda(k))^{-1}$$

where

$$\hat{Z}(\lambda(k)) = \sum_{i=1}^{4} \lambda_i(k) Z_{i,1}$$
$$\hat{G}(\lambda(k)) = \sum_{i=1}^{4} \lambda_i(k) G_{i,1}. \tag{13}$$

This control is proved to stabilize affine parameter-dependent systems such as (9) with a guaranteed $\mathcal{H}_2$ and $\mathcal{H}_\infty$ performance for all $\lambda \in \Lambda$ and $|\Delta\lambda| \leq b$. In this work, to ensure that all possible parameter variations would be covered, we selected $b = 0.4$. The LMI conditions of Theorems 8 and 9 of [13] are solved by programming them into MATLAB using the LMI parser YALMIP [17] and solved using SeDuMi [18]. During the solution process, the goal is to calculate the gain-scheduled feedback controller $K(\lambda(k))$ that minimizes the bound ν on the $\mathcal{H}_2$ performance from $w(k)$ to $[z_3, z_4, z_5]^\mathsf{T}$ under a prescribed bound η on the $\mathcal{H}_\infty$ norm from $w(k)$ to $[z_1, z_2]^\mathsf{T}$. The procedure for performing the mixed $\mathcal{H}_2/\mathcal{H}_\infty$ control synthesis is outlined in Algorithm 1.

Algorithm 1 Mixed $\mathcal{H}_2/\mathcal{H}_\infty$ Gain-Scheduling Synthesis

Input: Polytopic LPV system in **(9)**, rate of variation bound $b \in [0, 1]$, $\mathcal{H}_2$ and $\mathcal{H}_\infty$ input and output channels of **(9)**, and a range of prescribed $\mathcal{H}_\infty$ bounds $\eta \in [\eta_L, \eta_U]$, where it is assumed that η_L is the minimum feasible $\mathcal{H}_\infty$ bound.

Output: The gain-scheduling controller matrices $G_{i,1}$ and $Z_{i,1}$ needed to compute $K(\lambda(k))$ in **(13)**.

1: Determine selection matrices L_j and M_j for each performance specification j as in Section 5.3 of **[13]**.

2: Compute H_j using selection matrices L_j and M_j for each performance specification j, for $j = 1, 2$.

3: Compute the vectors f^j and h^j using rate of variation bound b as shown in Appendix 11.3 of **[13]**.

4: Using equation (28) of **[13]**, convert the polytopic LPV system in **(9)** to the form used in the LMIs of Theorems 8 and 9 of **[13]**.

5: **for** $\eta = \eta_L{:}\eta_U$ **do**

6: Initialize the matrix variables introduced in Theorems 8 and 9 of **[13]** as free matrix variables into MATLAB using the YALMIP interface **[17]**.

7: Using G_{i,K_s}, $G_{i,L}$, Z_{i,K_s}, and $Z_{i,L}$, generate $G_{i,1}$ and $Z_{i,1}$ as shown in **(12)**.

8: Using the YALMIP interface **[17]**, program the $\mathcal{H}_\infty$ LMIs in Theorem 8 of **[13]** using prescribed bound η and the $\mathcal{H}_2$ LMIs in Theorem 9 of **[13]** into MATLAB.

Fig. 4. VVT phase actuator test bench.

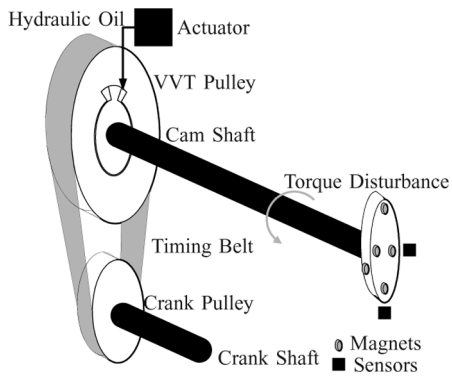

Fig. 5. VVT phase actuator test bench diagram.

9: Using an LMI solver, like SeDuMi **[18]**, solve the system of LMIs with the objective of minimizing $\sum_{i=1}^{4} Tr\{W_i\}$, where W_i is a positive-definite $\mathcal{H}_2$ free matrix variable introduced in Theorem 9 of **[13]**, thus minimizing the $\mathcal{H}_2$ norm.

10: **end for**

11: Select the solution that minimizes the $\mathcal{H}_2$ norm the most, yet still has an acceptable bound η on the $\mathcal{H}_\infty$ norm.

Note that the minimum feasible $\mathcal{H}_\infty$ bound η_L can be solved for by using an iterative algorithm [15], such as the bisection algorithm.

The resulting LPV controller solved at an engine speed and oil pressure of $N = 1500$ rpm and $p = 414$ kPa (for comparison with the $\mathcal{H}_2$ output covariance controller) is found to be

$$K_{\mathrm{LPV}}(q) = \frac{a_1 q^3 + a_2 q^2 + a_3 q + a_4}{q^4 + a_5 q^3 + a_6 q^2 + a_7 q + a_8}. \tag{14}$$

As stated previously, the robust $\mathcal{H}_2$ controller designed in [4] using the OCC control design algorithm presented in [5] is used for comparison with the LPV controller. The robust $\mathcal{H}_2$ OCC controller designed in [4] is given by

$$K_{\mathrm{OCC}}(q) = \frac{b_1 q^3 + b_2 q^2 + b_3 q + b_4}{q^4 + b_5 q^3 + b_6 q^2 + b_7 q + b_8}. \tag{15}$$

The coefficients a_i and b_i of K_{LPV} and K_{OCC} are given in Table III.

TABLE III
COEFFICIENTS OF THE LPV AND OCC CONTROLLERS

	1	2	3	4	5	6	7	8
a_i	0.109255247	-0.302866405	0.278279285	-0.0846677044	-3.132121334	3.625898107	-1.853079890	0.359303117
b_i	0.3158302	-0.9301618	0.9129406	-0.2986088	-3.4051293	4.3533113	-2.4909563	0.5427743

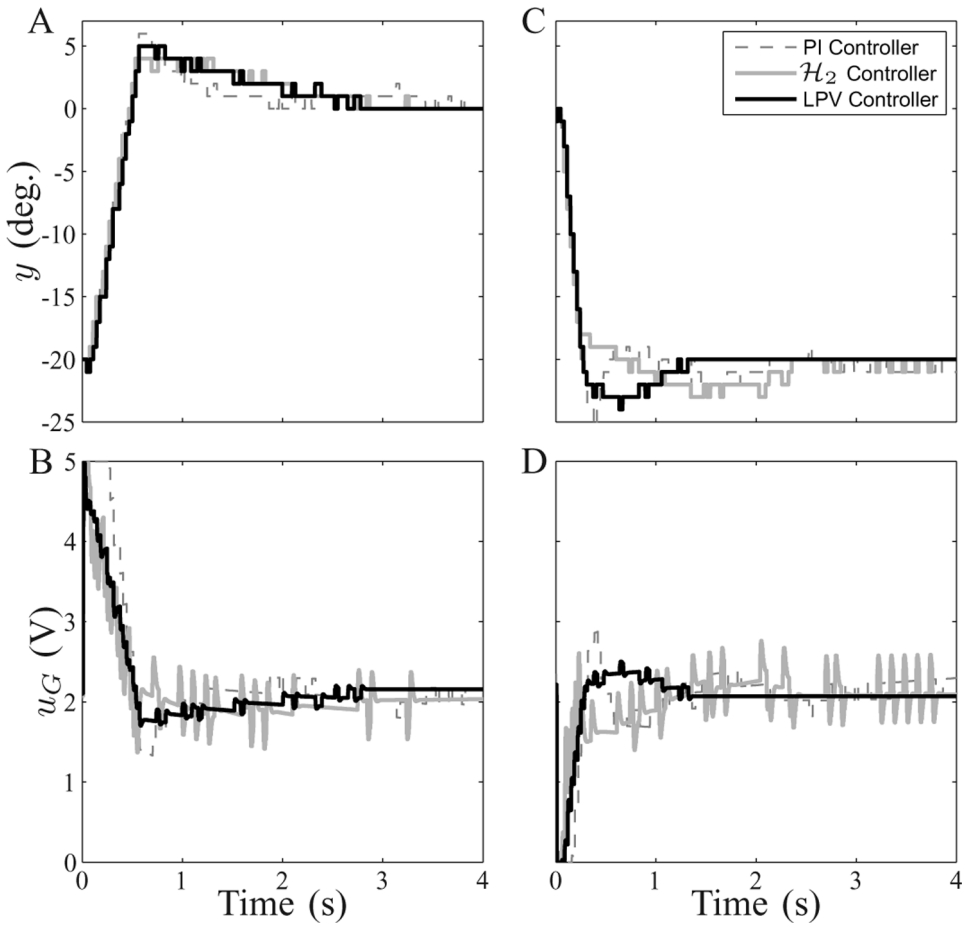

Fig. 6. Cam advance response at 900 rpm with 310 kPa oil pressure.

IV. VVT SYSTEM TEST BENCH

A. Bench Test Setup

The closed-loop system identification outlined in [4] and the control design testing were conducted on the VVT test bench displayed in Fig. 4. A Ford 5.4L V8 engine head was modified and mounted on the test bench. The cylinder head has a single cam shaft with a VVT actuator for one exhaust and two intake valves. These valves introduce a cyclic torque disturbance to the cam shaft. The cam shaft is driven by an electrical motor (simulating the crankshaft) through a timing belt, see Fig. 5.

An encoder is installed on the motor shaft, which generates the crank angle signal with one degree resolution, along with a so-called gate signal (one pulse per revolution). A plate with five magnets adhered is mounted at the other side of the extended cam shaft. As displayed in Fig. 5, one magnet is placed on the edge of the plate and is used to synchronize the top dead center position of the combustion phase. The other four magnets on the face of the plate are used to determine the cam phase four times per engine cycle. The two squares in Fig. 5 represent hall-effect cam position sensors. As the cam shaft rotates, the magnets on the plate face pass the hall-effect cam position sensor used to to determine cam phase and the magnet on the edge of the plate passes the hall-effect cam position sensor used to determine top dead center position. Within an engine cycle, the cam position sensor generates four cam position pulses, which are sampled by an Opal-RT real-time controller. By comparing these pulse locations with respect to the encoder gate signal, the Opal-RT controller calculates the cam phase with one crank degree resolution.

The cam phase actuator system consists of a solenoid driver circuit, a solenoid actuator, and a hydraulic cam actuator. The solenoid actuator is controlled by a pulse-width modulation (PWM) signal, whose duty cycle is linearly proportional to the DC voltage command. An electrical oil pump was used to supply pressurized engine oil to be used for lubrication and as hydraulic actuating fluid for the cam phase actuator. The cam actuator command voltage signal is generated by the Opal-RT prototype controller and sent to the solenoid driver. The PWM duty cycle is linearly proportional to input voltage with a maximum duty cycle 99% corresponding to 5 V and a minimal duty cycle of 1% corresponding to 0 V. The solenoid actuator

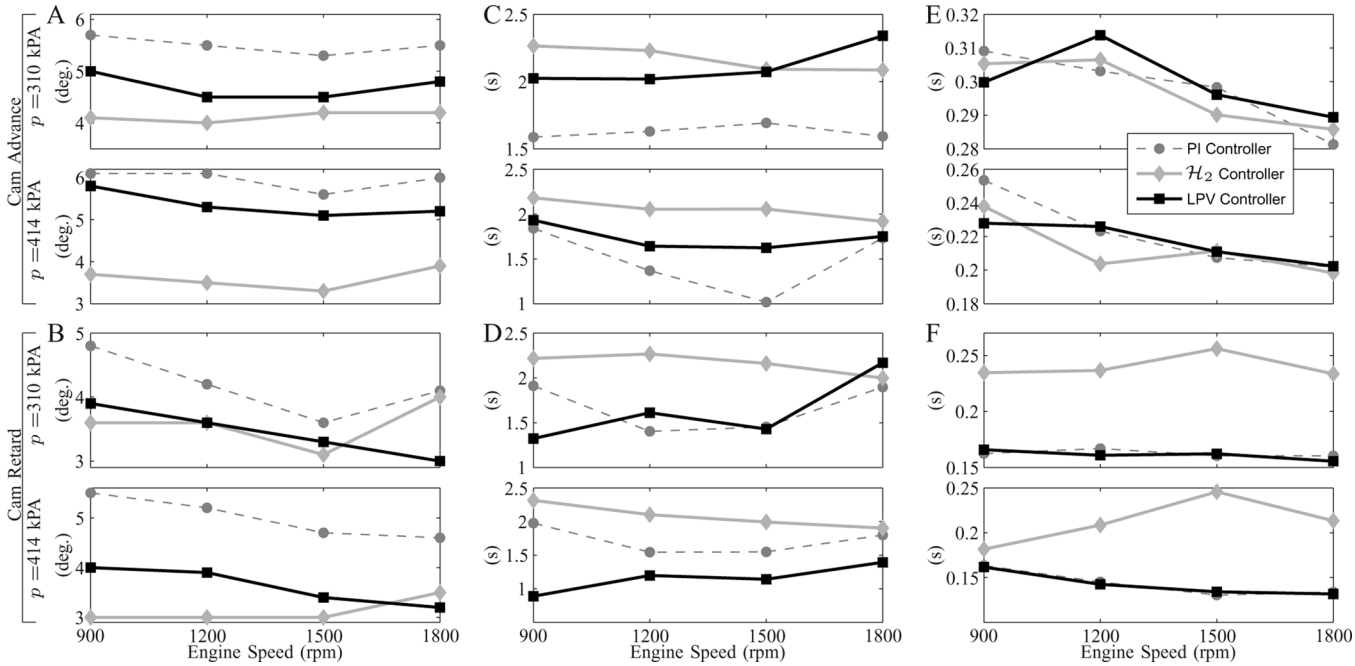

Fig. 7. Mean overshoot, 5% settling time, and 10 to 90% rising time for each controller operated at oil pressures of 310 and 414 kPa and engine speeds of 900, 1200, 1500, and 1800 rpm.

controls the hydraulic fluid (engine oil) flow and changes the cam phase. The cam position sensor signal is sampled by the Open-RT prototype controller and the corresponding cam phase is calculated within the Opal-RT real-time controller.

A PI controller was tuned for the VVT system on the test bench for comparison purpose with the LPV and OCC controllers. The PI gains tuning process was completed at different engine speeds and oil pressures. The following tuned PI controller achieves good balance between response time and overshoot oscillations at different conditions:

$$K_{PI}(q) = \frac{0.2q - 0.1995}{q - 1}. \tag{16}$$

B. Bench Test Results

The mixed $\mathcal{H}_2/\mathcal{H}_\infty$ observer-based dynamic LPV controller was tested on the VVT cam phaser bench at engine speeds of 900, 1200, 1500, and 1800 rpm for both engine oil pressures of 310 and 414 kPa. The step response of each controller is displayed in Fig. 6 for the cam advance (-20° to 0°) and the cam retard (0° to -20°) at an engine speed of 900 rpm and an oil pressure of 310 kPa. In Fig. 6(b), the control effort of both the LPV and $\mathcal{H}_2$ controllers is visibly lower than the PI controller. Also noticeable in Fig. 6(b) is that the control effort corrections produced by the LPV controller are smaller than those produced by the $\mathcal{H}_2$ controller. This was anticipated from frequency response plot of each controller in Fig. 3(a). Since the LPV controller has lower gain than the $\mathcal{H}_2$ controller, it is less sensitive to the change in error signal (which has the resolution of one crank degree in the experiment), which makes the LPV controller more robust to disturbances in the cam phase when compared to the $\mathcal{H}_2$ controller. This is even more noticeable during cam retard in Fig. 6(c) and (d). The performance of the LPV controller in comparison with the $\mathcal{H}_2$ and PI controllers can also be shown by computing the control variance once the cam phase has reached steady state. During cam advance with an engine speed of 900 rpm and oil pressure of 310 kPa, the control variances of the LPV, $\mathcal{H}_2$, and PI controllers were found to be 0.0048 V^2, 0.0265 V^2, and 0.0079 V^2, respectively. During cam retard at the same engine conditions, the control variances of the LPV $\mathcal{H}_2$ and PI controllers were found to be 0.0063 V^2, 0.0281 V^2, and 0.0068 V^2, respectively. Similar values for the control variance for each controller were found at all other engine conditions tested as well. The control variances of the LPV controller under all engine conditions tested were found to be approximately anywhere from 6% to 33% of the control variance of the $\mathcal{H}_2$ controller.

In Fig. 7, the mean of the measured overshoot, 5% settling time, and 10% to 90% rising time from ten test runs at each engine condition is plotted for each controller. It is easy to see from Fig. 7(a) and (b), that in all cases both the $\mathcal{H}_2$ controller and LPV controller obtain lower overshoot than the PI controller, with the $\mathcal{H}_2$ controller displaying the lowest overshoot in most cases. However, during the cam retard situation displayed in Fig. 7(b), the overshoot of the LPV controller is much closer to that of the $\mathcal{H}_2$ controller and is even smaller than the $\mathcal{H}_2$ controller at an engine speed of 1800 rpm. The difference in performance between cam advance and cam retard is attributed to the fact that the dynamics are slightly different. During cam advance, the actuating torque generated by the oil pressure overcomes the cam load torque causing the cam phase to advance. However, during cam retard, the oil trapped inside the actuator bleeds back to the oil reserve when the cam phase is pushed back by the cam load shaft. This difference in dynamics between the cam advance and cam retard, as shown in Fig. 7(a) and (b), generally results in

lower overshoot and faster settling and rising times for the cam retard performance compared to the cam advance performance. We note here that while the overshoot performance of all of the controllers in Fig. 7(a) and (b) is above 15%, none of the controllers include feedforward control. With feedforward control the overshoot would be significantly reduced.

In Fig. 7(c) and (d), it is observed that for nearly all cases the LPV controller settles quicker than the $\mathcal{H}_2$ controller, with one exception of when the engine is operated with an oil pressure of 310 kPa and at an engine speed of 1800 rpm. For the cam advance, the PI controller almost uniformly has the quickest settling time. However, as observed in Fig. 7(d), during cam retard the settling time of the LPV controller is quicker than the PI controller in most cases, especially when the engine oil pressure is 414 kPa.

The rising time performance during cam advance is very similar for each of the controllers as displayed in Fig. 7(e). However, as shown in Fig. 7(f), during cam retard it is quite clear that the LPV and PI controllers are faster than the $\mathcal{H}_2$ controller by an unmistakable amount.

V. Conclusion

In this paper, a dynamic gain-scheduling controller was designed by employing an observer-based state feedback design and static multi-objective $\mathcal{H}_2/\mathcal{H}_\infty$ controller synthesis. By examining the frequency response of the LPV controller and comparing it to a previously obtained robust $\mathcal{H}_2$ OCC controller, the LPV controller was found to reduce the operating bandwidth variation of the closed-loop system by approximately 60%. The frequency response of each system also demonstrated that the LPV controller had lower control effort over the crucial frequency range of 1–20 Hz. This was validated by the bench tests run with each controller, which showed that the LPV controller had much lower control variance than the robust $\mathcal{H}_2$ OCC controller. Also, while the LPV controller is more complex than the PI controller in both concept and implementation, it has lower overshoot than the PI controller at all operating conditions with similar settling and response time characteristics. Additionally, the LPV controller was designed with a systematic approach while the PI controller was obtained through ad hoc testing.

Appendix
State Space Matrices

The output and feedthrough state-space matrices of (6) and (9) are

$$C_z = \begin{bmatrix} 0 & 1 & 0 & 0 & 0 & 0 \\ 0 & 0 & -10\sqrt{t_s} & 0 & 0 & 0 \\ 0 & 1 & 0 & 0 & 0 & 0 \\ 0 & 0 & 0 & 0 & 0 & 0 \\ 0 & 0 & 0 & 0 & 0 & 0 \end{bmatrix}$$

$$D_w = \begin{bmatrix} 1 \\ 0 \\ 1 \\ 0 \\ 0 \end{bmatrix}$$

$$D_u = \begin{bmatrix} 0 & 0 & 0 & 0 & 0 \\ -10 & 0 & 0 & 0 & 0 \\ 0 & 0 & 0 & 0 & 0 \\ 15 & 0 & 0 & 0 & 0 \\ 0 & 15 & 0 & 0 & 0 \end{bmatrix}$$

$$C_e = \begin{bmatrix} 0 & 0 & 0 & 1 & 0 & 0 \\ 0 & 0 & 0 & 0 & 1 & 0 \\ 0 & 0 & 0 & 0 & 0 & 1 \\ 0 & -1 & 0 & 0 & 1 & 0 \end{bmatrix}.$$

References

[1] Y. Moriya, A. Watanabe, H. Uda, H. Kawamura, M. Yoshiuka, and M. Adachi, "A newly developed intelligent variable valve timing system—Continuously controlled cam phasing as applied to new 3 liter inline 6 engine," SAE, Warrendale, PA, 960579, 1996.

[2] P. H. Dugdale, R. J. Rademacher, B. R. Price, J. W. Subhedar, and R. L. Duguay, "Ecotec 2.4L VVT: A variant of GM's global 4-cylinder engine," SAE, Warrendale, PA, 2005-01-1941, 2005.

[3] A. Genç, K. Glover, and R. Ford, "Nonlinear control of hydraulic actuators in variable cam timing engines," presented at the MECA Int. Workshop, Salerno, Italy, 2001.

[4] Z. Ren and G. G. Zhu, "Integrated system ID and control design for an IC engine variable valve timing system," *ASME J. Dyn. Syst., Meas. Control*, vol. 133, no. 2, 2010.

[5] G. Zhu, M. Rotea, and R. E. Skelton, "A convergent algorithm for the output covariance constraint control problem," *SIAM J. Control Opt.*, vol. 35, pp. 341–361, 1997.

[6] X. Wei and L. del Re, "Gain scheduled $\mathcal{H}_\infty$ control for air path systems of diesel engines using LPV techniques," *IEEE Trans. Control Syst. Technol.*, vol. 15, no. 3, pp. 406–415, May 2007.

[7] J. Salcedo and M. Martínez, "LPV identification of a turbocharged diesel engine," *Appl. Numer. Math.*, vol. 58, pp. 1553–1571, 2008.

[8] R. A. Zope, J. Mohammadpour, K. M. Grigoriadis, and M. Franchek, "Air-fuel ratio control of spark ignition engines with TWC using LPV techniques," in *Proc. ASME Dyn. Syst. Control Conf.*, 2009, pp. 897–903.

[9] F. Zhang, K. M. Grigoriadis, M. A. Franchek, and I. H. Makki, "Linear parameter-varying lean burn air-fuel ratio control for a spark ignition engine," *J. Dyn. Syst., Meas. Control*, vol. 192, pp. 404–414, 2007.

[10] A. White, J. Choi, R. Nagamune, and G. Zhu, "Gain-scheduling control of port-fuel-injection processes," *IFAC J. Control Eng. Pract.*, vol. 19, pp. 380–394, 2010.

[11] A. White, G. Zhu, and J. Choi, "Hardware-in-the-loop simulation of robust gain-scheduling control of port-fuel-injection processes," *IEEE Trans. Control Syst. Technol.*, vol. 19, no. 6, pp. 1433–1443, Nov. 2010.

[12] Z. Ren and G. Zhu, "Pseudo-random binary sequence closed-loop system identification error with integration control," *Proc. Inst. Mechan. Eng., I, J. Syst. Control Eng.*, vol. 223, no. 6, pp. 877–884, 2009.

[13] J. Caigny, J. Camino, R. Oliveira, P. Peres, and J. Swevers, "Gain scheduled $\mathcal{H}_2$ and $\mathcal{H}_\infty$ control of discrete-time polytopic time-varying systems," *IET Control Theory Appl.*, vol. 4, pp. 362–380, 2010.

[14] K. Zhou and J. C. Doyle, *Essentials of Robust Control*. Englewood Cliffs, NJ: Prentice-Hall, 1998.

[15] S. Skogestad and I. Postlethwaite, *Multivariable Feedback Control: Analysis and Design*, 2nd ed. New York: Wiley, 2005.

[16] J. Warren, S. Schaefer, A. N. Hirani, and M. Desbrun, "Barycentric coordinates for convex sets," *Adv. Comput. Math.*, vol. 27, no. 3, pp. 319–338, 2007.

[17] J. Löfberg, "Yalmip: A toolbox for modeling and optimization in MATLAB," presented at the CACSD Conf., Taipei, Taiwan, 2004. [Online]. Available: http://users.isy.liu.se/johanl/yalmip

[18] J. Sturm, "Using SeDuMi 1.02, a MATLAB toolbox for optimization over symmetric cones," *Optimization Methods Softw.*, vol. 11, no. 1, pp. 625–653, 1999.

Andrew White (S'10) received the B.S. and M.S. degrees in mechanical engineering from Michigan State University, East Lansing, in 2006 and 2008, respectively, where he is currently pursuing the Ph.D. degree from the Department of Mechanical Engineering, Michigan State University.

His research interests include adaptive and robust control, and parameter estimation, with applications to engine control, robotics, and non-destructive testing and evaluation.

Zhen Ren received the B.S. degree in automotive engineering from Tongji University, Shanghai, China, in 2002, and the M.S. degree in mechanical engineering from Michigan State University, East Lansing, in 2008, where he is currently pursuing the Ph.D. degree in mechanical engineering.

From 2002 to 2006, he was a Vehicle Dynamics Engineer with Pan Asia Technical Automotive Center, Shanghai. His research interests are dynamic system modeling, and control applications for automotive systems.

Guoming Zhu received the B.S. and M.S. degrees from Beijing University of Aeronautics and Astronautics, Beijing, China, in 1982 and 1984, respectively, and the Ph.D. degree in aerospace engineering from Purdue University, West Lafayette, IN, in 1992.

He is an Associate Professor with the Department of Mechanical Engineering (ME), and Electrical and Computer Engineering (ECE), Michigan State University, East Lansing. Prior to joining the ME and ECE Departments, he was a Technical Fellow with Advanced Powertrain Systems, Visteon Corporation. He also worked for Cummins Engine Co., Ltd. His teaching interests focus on control classes at both undergraduate and graduate levels; and his current research interests include closed-loop combustion control of internal combustion (IC) engines, engine system modeling and identification, hybrid powertrain control and optimization, etc. He has over 24 years of experience related to control theory, engine diagnostics, and combustion control. He has authored or coauthored over 100 refereed technical papers and holds 40 U.S. patents.

Dr. Zhu is an ASME fellow and was an Associate Editor for the *ASME Journal of Dynamic Systems, Measurement, and Control*.

Jongeun Choi (S'05–M'06) received the Ph.D. and M.S. degrees in mechanical engineering from the University of California at Berkeley, in 2006 and 2002, respectively, and the B.S. degree in mechanical design and production engineering from Yonsei University, Seoul, Korea, in 1998.

He is currently an Assistant Professor with the Department of Mechanical Engineering and the Department of Electrical and Computer Engineering, Michigan State University, East Lansing. His research interests include adaptive, distributed and robust control and statistical learning algorithms, with applications to mobile robotic sensors, environmental adaptive sampling, engine control, and biomedical problems.

Prof. Choi was a recipient of an NSF CAREER Award in 2009. His papers were finalists for the Best Student Paper Award at the 24th American Control Conference (ACC) 2005 and the Dynamic System and Control Conference (DSCC) 2011. He is a member of the ASME.